

1 Article

2 Monitoring and Forecasting the Impact of the 2018 3 Summer Heatwave on Vegetation

4 Clément Albergel¹, Emanuel Dutra², Bertrand Bonan¹, Yongjun Zheng¹, Simon Munier¹,
5 Gianpaolo Balsamo³, Patricia de Rosnay³, Joaquin Munoz-Sabater³ and Jean-Christophe Calvet¹

6 ¹ CNRM - Université de Toulouse, Météo-France, CNRS, Toulouse, France

7 ² Instituto Dom Luiz, IDL, Faculty of Sciences, University of Lisbon, Portugal

8 ³ ECMWF, Reading, UK

9 * Correspondence: clement.albergel@meteo.fr

10 **Abstract:** This study aims to assess the potential of the LDAS-Monde platform, a land data
11 assimilation system developed by Météo-France, to monitor the impact on vegetation state of the
12 2018 summer heatwave over western Europe. The LDAS-Monde is forced by the ECMWF's (i)
13 ERA5 reanalysis, and (ii) the Integrated Forecasting System High Resolution operational analysis
14 (IFS-HRES), used in conjunction with the assimilation of Copernicus Global Land Service (CGLS)
15 satellite-derived products, namely the Surface Soil Moisture (SSM) and the Leaf Area Index (LAI).
16 Analysis of long time series of satellite derived CGLS LAI (2000-2018) and SSM (2008-2018)
17 highlights marked negative anomalies for July 2018 affecting large areas of northwestern Europe
18 and reflects the impact of the heatwave. Such large anomalies spreading over a large part of the
19 considered domain have never been observed in the LAI product over this 18-yr period. The
20 LDAS-Monde land surface reanalyses were produced at spatial resolutions of 0.25°x0.25° (January
21 2008 to October 2018) and 0.10°x0.10° (April 2016 to December 2018). Both configurations of the
22 LDAS-Monde forced by either ERA5 or HRES capture well the vegetation state in general and for
23 this specific event, with HRES configuration exhibiting better monitoring skills than ERA5
24 configuration. The consistency of ERA5 and IFS HRES driven simulations over the common period
25 (April 2016 to October 2018) allowed to disentangle and appreciate the origin of improvements
26 observed between the ERA5 and HRES. Another experiment, down-scaling ERA5 to HRES spatial
27 resolutions, was performed. Results suggest that land surface spatial resolution is key (e.g.
28 associated to a better representation of the land cover, topography) and using HRES forcing still
29 enhance the skill. While there are advantages in using HRES, there is added value in down-scaling
30 ERA5, which can provide consistent, long term, high resolution land reanalysis. If the
31 improvement from LDAS-Monde analysis on control variables (soil moisture from layers 2 to 8 of
32 the model representing the first meter of soil and LAI) from the assimilation of SSM and LAI was
33 expected, other model variables benefit from the assimilation through biophysical processes and
34 feedbacks in the model. Finally, we also found added value of initializing 8-day land surface HRES
35 driven forecasts from LDAS-Monde analysis when compared with model-only initial conditions.

36 **Keywords:** land surface modelling; data assimilation; Leaf Area Index; Surface Soil Moisture;
37 Summer 2018 heatwave
38

39 1. Introduction

40 Land surface conditions are critical in the global weather and climate system. Accurate
41 characterization and simulation of hydrological and biophysical variables at the land surface
42 represent a significant challenge given large spatial heterogeneity and human modifications of the
43 land surface. In particular, observing and simulating the response and feedbacks of land surface

44 conditions to extreme events is crucial in our ability to manage adaptation to climate change
45 impacts. Land Surface Model (LSM)'s role has evolved over the years, from the primary goal of
46 providing boundary conditions to atmospheric models to being used as monitoring and forecasting
47 tools for estimating land surface conditions [1-4]. Modelling of terrestrial variables can be improved
48 through the dynamical integration of observations [5-7] and there is a growing emphasis on
49 constraining the LSM estimates with observational inputs as well as coupling them with other
50 models of the Earth system [8-9, 10, 1]. Enhanced estimates of land surface conditions are also
51 recognized to lead towards improved forecasts of weather patterns, sub-seasonal temperatures and
52 precipitations, agricultural productivity, seasonal streamflow, floods and droughts as well as carbon
53 cycle [11-16]. Remote sensing observations are particularly useful in this context as they are now
54 unrestrictedly available at a global scale with high spatial resolution and with long-term records.
55 Many satellite-derived products relevant to the hydrological (e.g. soil moisture, snow depth/cover,
56 terrestrial water storage), vegetation (e.g. leaf area index, biomass) and energy (e.g. land surface
57 temperature, albedo) cycles are readily available [17]. Data assimilation techniques allow to spatially
58 and temporally integrate the observed information into LSMs in a consistent way [5, 18]. We refer to
59 Land Data Assimilation Systems (LDASs) as the framework where LSMs are driven by and/or ingest
60 such observations generating enhanced estimates of the land surface variables (LSVs) [10]. Several
61 LDASs now exist from point to regional scale, amongst them are the Global Land Data Assimilation
62 System (GLDAS, [19]), the Carbon Cycle Data Assimilation System (CCDAS, [20]), the Coupled
63 Land Vegetation LDAS (CLVLDAS, [21-22]) and more recently the U.S. National Climate Assessment
64 LDAS (NCA-LDAS, [10]) as well as LDAS-Monde [7, 18] to name a few. These LDASs either
65 optimize process parameters (e.g. CCDAS), state variables (e.g. GLDAS, NCA-LDAS, LDAS-Monde)
66 or both (e.g., CLVLDAS). Assimilated Earth Observations (EOs) generally include satellite retrieval
67 of surface soil moisture [5, 8, 23-25], snow depth [26-29] and snow cover [30-31, 9, 27], vegetation
68 [32-35, 7, 18], as well as terrestrial water storage [36-38]. Few studies have included multiple remote
69 sensing measurements. For instance, [10] assimilates various remote sensing measurements of the
70 terrestrial water cycle within the NCA-LDAS over the USA while LDAS-Monde [7, 18] considers the
71 joint assimilation of vegetation (Leaf Area Index, LAI) and surface soil moisture (SSM)
72 measurements. LDAS-Monde is a sequential land data assimilation system with global capacity. It
73 has been evaluated over various domains at various spatial resolutions including France at 8 km
74 scale [33, 39] forced by the SAFRAN reanalysis of Météo-France (Système d'Analyse Fournissant des
75 Renseignements Atmosphériques à la Neige, [40-41], Europe at 0.5°x0.5° [18, 35] forced by
76 ERA-Interim atmospheric reanalysis from the European Center For Medium Range Weather
77 Forecast (ECMWF) [42], North America [7] and Burkina-Faso in western Africa at 0.25°x0.25° [43]
78 forced by ERA5 atmospheric reanalysis [44]. In those studies, analysis impact was successfully
79 evaluated using several datasets such as (i) in situ measurements of soil moisture (ii) agricultural
80 statistics, (iii) river discharge, (iv) independent flux estimates related to vegetation dynamics
81 (evapotranspiration, Sun-Induced Fluorescence (SIF) and Gross Primary Productivity (GPP)).
82 Albergel et al., [7], highlighted LDAS-Monde capacity to better characterize agricultural droughts
83 (spatial area and intensity) than an open-loop counterpart (i.e. model without any assimilation of
84 satellite derived measurements) over the continental United States of America. They found that
85 LDAS-Monde can provide improved initial conditions to initialize forecast and that its impacts
86 persist through time, also. In the above mentioned study, LDAS-Monde satellite-derived surface soil
87 moisture dataset (ESA CCI SSM, [45-48]) along with satellite derived LAI (GEOV1,
88 <http://land.copernicus.eu/global/> last access, June 2018), were jointly assimilated leading to a quarter
89 degree spatial resolution reanalysis of the LSVs over 2010-2016.

90 Stemming from previous work [7], the present study investigates the capability of
91 LDAS-Monde to represent the impact of the summer 2018 heatwave in Europe on vegetation. Spring
92 and summer 2018 in Europe were marked by unusually hot weather that has led to record-breaking
93 temperatures in many countries across northern and central Europe. According to ECMWF,
94 near-surface air temperature anomaly in Europe in the period of April to August, calculated with
95 respect to the 1981–2010 average for those months, was much larger in 2018 than in any previous

96 year since 1979 [49]. According to the National Oceanic and Atmospheric Administration -NOAA-
97 Europe had its second warmest July on record. It follows its second warmest June on record (behind
98 2003), its warmest May since continental records began in 1910, surpassing the previous record set in
99 2003: the whole summer 2018 was Europe's warmest since continental records began in 1910 at
100 +2.16°C (Global Climate Report, <https://www.ncdc.noaa.gov/sotc/global/>, last access October 2018).
101 Northern Hemisphere summer precipitation was generally weaker than normal across central
102 Europe.

103 Such an event is likely to affect land surface conditions. In this study, satellite derived estimates
104 of LAI and SSM as well as LDAS-Monde are used to monitor the impact of the heatwave on
105 vegetation, focusing on July 2018. Firstly, we assess the heatwave impact on satellite derived LAI and
106 SSM, using time-series over 2000 to 2018 and 2008 to 2018, respectively. Secondly, we evaluate the
107 heatwave impact on the simulated LAI from LDAS-Monde forced by ECMWF ERA-5 reanalysis
108 from January 2008 to October 2018 at 0.25°x0.25° and by ECMWF Integrated Forecasting System (IFS)
109 high resolution operational analysis (HRES) from April 2016 to December 2018 at 0.10°x0.10°. The
110 use of both ERA5 and HRES to force LDAS-Monde enable to assess the impact of resolution versus
111 system quality over a common one year period (2017) were ERA5 was downscaled to HRES spatial
112 resolution. Another added value of using HRES consists in its forecast capacity, up to 10 days ahead.
113 Forecast of LAI initialized by LDAS-Monde analysis with a leading time up to 8-days is then
114 investigated in order to assess whether or not the heatwave impact on land surface conditions could
115 have been anticipated. The remainder of this paper is organized as follows: section 2 describes the
116 LDAS-Monde system, the satellite derived estimates of LAI and SSM and the ECMWF analysis and
117 reanalysis forcing, results are analyzed and discussed in sections 3 and 4.

118 2. Material and Methods

119 This study assesses the ability of LDAS-Monde sequential assimilation of satellite derived
120 surface SSM and LAI to represent the impact of the summer 2018 heatwave in Europe on vegetation.
121 The following sections describe LDAS-Monde system as well as 2 other key elements of its setup:
122 atmospheric forcing (LDAS-Monde being an offline system) and satellite derived observations.

123 2.1. LDAS-Monde

124 Within the SURFEX modelling platform of Météo-France (Surface Externalisée, [50], Version
125 8.1), the LDAS [32-33, 34, 39, 51] developed in the research department of Météo-France, the CNRM
126 (Centre National de Recherches Météorologiques) permits integrating satellite products into the
127 ISBA LSM [52-55] using a data assimilation scheme. The LDAS was extended to a global scale
128 (LDAS-Monde, [18]). At the same time, the coupling to hydrological models (ISBA-CTRIP for
129 ISBA-CNRM-, Total Runoff Integrating Pathways) was consolidated. A full description of the
130 ISBA-CTRIP system is presented in [56]. The obtained land surface reanalyses from LDAS-Monde
131 account for the synergies of the various upstream products (e.g., model and satellite derived
132 observations) and are able to provide an improved representation of the LSVs, as well as statistics
133 which can be used to monitor the quality of the assimilated observations (e.g. [7], [18], [35]).
134 LDAS-Monde can also be used to calibrate model parameters (e.g., [57] for the soil maximum
135 available water content within ISBA).

136 LDAS-Monde uses the CO₂-responsive [53-55], multi-layer soil [56-59], version of ISBA. The
137 later allows to solve the energy and water budgets at the surface level and describes the exchanges
138 between the land surface and the atmosphere. Parameters of the ISBA LSM are defined for 12
139 generic land surface patches: nine plant functional types (namely: needle leaf trees, evergreen
140 broadleaf trees, deciduous broadleaf trees, C3 crops, C4 crops, C4 irrigated crops, herbaceous,
141 tropical herbaceous, and wetlands) as well as bare soil, rocks, and permanent snow and ice surfaces.
142 They are derived from ECOCLIMAP-II, the land cover map used in SURFEX [60]. Atmospheric and
143 climate conditions drive the dynamic evolution of the vegetation biomass and LAI through
144 vegetation growth and mortality processes implemented in the form of a nitrogen dilution process

145 -NIT option- [53, 55, 61]. Photosynthesis enables vegetation growth resulting from the CO₂ net
146 assimilation. During the growing phase, enhanced photosynthesis corresponds to a CO₂ net
147 assimilation, which results in vegetation growth from the LAI minimum threshold (1 m² m⁻² for
148 coniferous forest or 0.3 m² m⁻² for other vegetation types). Vegetation phenology relies on
149 photosynthesis-driven plant growth and mortality, and photosynthesis is related to the mesophyll
150 conductance. More information on the CO₂-responsive version of ISBA can be found in [62-63], also.

151 The multilayer diffusion scheme described in [58-59] drives transfers of water and heat through the
152 soil. Finally, the Simplified Extended Kalman Filter Data Assimilation (DA) technique (SEKF, [18,
153 32-33, 34, 39, 51] is the main technique available within LDAS-Monde. While ensemble based DA
154 techniques are currently being tested and implemented [39, 64], to date the LDAS-Monde SEKF is
155 the more robust. It uses finite differences to compute the flow dependency between the assimilated
156 observations (SSM and LAI) and the analyzed variables (soil moisture from soil layer 2 (1cm to 4cm)
157 to layer 8 (80cm to 100cm), representing the first meter of soil and LAI, see Table I). Further details of
158 the analysis methodology can be found in [34, 18]. While control variables are directly updated
159 thanks to their sensitivity to the observed variables, expressed by the SEKF Jacobians [18, 65], other
160 variables are indirectly modified by the analysis through biophysical processes and feedbacks in the
161 model by updates of the control variables.

Table I: Set up of the experiments used in this study.

Experiments (time period)	Model	Domain & spatial resolution	Atm. forcing	DA method	Assimilated observations	Observations operators	Control variables
LDAS-ERA5 (2008-10/2018)	ISBA Multi-layer soil model CO ₂ -responsive version (Interactive vegetation)	Western Europe defined as longitudes from 10.5°W to 20.5°E, latitudes from 42°N to 59°N	ERA5	SEKF	SSM (ASCAT)	Rescaled WG2 (Second layer of soil (1-4cm))	Layers of soil 2 to 8 (WG2 to WG8, 1-100cm) LAI
LDAS_HRES (04/2016-2018 2018)			IFS_HRES		LAI (GEOV2)	LAI	
ERA5_010 (2017)		ERA5 downscaled to 0.10°x0.10°	12-month model run				
LDAS_fc_d2 (2018)		IFS_HRES day 2 forecast	12-month model run, every day a 2-day forecast initialized by an analysis is ran				
LDAS_fc_d8 (2018)	IFS_HRES day 8 forecast	12-month model run, every day an 8-day forecast initialized by an analysis is ran					

164 2.2. *Satellite derived observations*

165 Two satellite products from the Copernicus Global Land Service project are used in this study,
166 the Surface Soil Moisture (SSM) and the Leaf Area Index (LAI) derived from SPOT-VGT (prior to
167 2014) and PROBA-V (from 2014 onward). The SSM is derived from the Advanced Scatterometer
168 (ASCAT), an active C-band microwave sensor on board the European MetOp polar-orbiting satellite
169 (METOP-A&B). Information on soil moisture comes from ASCAT radar backscatter coefficients
170 using a methodology developed at the Vienna University of Technology (TU-Wien) based on a
171 change detection approach originally developed for the active microwave instrument flown
172 on-board the European satellites ERS-1 and ERS-2 [66-67]. The recursive form on an exponential
173 filter [68] is applied to the soil moisture product to estimate the Soil Wetness Index (SWI) using a
174 timescale parameter, T, varying between 1 day and 100 days. The result for the top soil moisture
175 content (<5 cm) is expressed as a degree of saturation and ranges between 0 (dry) and 100
176 (saturated). In this study, SWI-001 (i.e. T=1 day) is used as a proxy for SSM [69]. It is a global product
177 at 0.1°x0.1° spatial resolution available daily from 2007. As in [7], pixels whose average altitude
178 exceeds 1500 m above sea level as well as pixels with urban land cover fractions larger than 15%
179 were discarded as those conditions may affect the retrieval of soil moisture from space. SSM product
180 has to be transformed into the model-equivalent surface soil moisture for data assimilation purposes
181 and in order to address possible misspecification of physiographic model parameters (like the field
182 capacity and the wilting point). Following [18] and [33] a linear re-scaling approach applied at a
183 seasonal scale over the whole considered periods was used. It makes use of the first two moments of
184 the cumulative distribution function (CDF) and consists of a linear re-scaling enabling a correction of
185 the differences in the mean and variance of the distribution.

186 LAI, defined as one-sided area of green elements of the canopy per unit horizontal ground area
187 is observable from space and practically quantifies the thickness of the vegetation cover. Several LAI
188 collections/versions are available from the CGLS project from 1999. They are retrieved from the
189 SPOT-VGT (from 1999 to 2014) and then from PROBA-V (from 2014 to present) satellite data
190 according to the methodology proposed by [70]. This study makes use of the GEOV2, 1km spatial
191 resolution and 10-day steps in near real time product. Its development has followed several steps
192 including (1) applications of a neural network for providing instantaneous estimates from
193 SPOT-VGT reflectances, (2) a multi-step filtering approach to eliminate contaminated data (e.g.,
194 affected by atmospheric effects and snow cover), and (3) temporal techniques for ensuring
195 consistency and continuity as well as short term projection of the product dynamics [71] (LAI
196 Product User Manual,
197 [https://land.copernicus.eu/global/sites/cgls.vito.be/files/products/GIOGL1_PUM_LAI300m-V1_I1.60](https://land.copernicus.eu/global/sites/cgls.vito.be/files/products/GIOGL1_PUM_LAI300m-V1_I1.60.pdf)
198 [.pdf](#), last access January 2019).

199 2.3. *ECMWF atmospheric forcing*

200 LDAS-Monde is driven by near-surface meteorological fields from both ECMWFs' reanalysis,
201 ERA5, released in 2018, as well as its high resolution operational high resolution weather analysis
202 and forecasts (HRES). ERA5 underlying model and data assimilation system are very similar to that
203 of the operational weather forecast. ERA5 production cycle (IFS Cycle 41r2) is still close to that of the
204 HRES (IFS Cycle 41r2 to 43r3 from 2016 and 45r1 from June 2018, more information at
205 <https://www.ecmwf.int/en/forecasts/documentation-and-support/changes-ecmwf-model>, last access January
206 2019). The main difference between the two is the horizontal resolution with 31 km in ERA5 and 9
207 km in HRES. Another difference is the data assimilation time window which is from 21:00 UTC to
208 09:00 UTC in ERA5 and from 21:00 UTC to 03:00 UTC in HRES, as it allows more observations to be
209 assimilated in ERA5. The shorter time window in HRES is due to ECMWF operational constraints to
210 deliver timely forecasts.

211 The ERA5 forcing data includes the lowest model level (about 10-meters height) air
212 temperature, wind speed, specific humidity and pressure and the downwelling fluxes of shortwave

213 and longwave radiation and precipitation partitioned in solid and liquid phases. ERA5 is processed
214 from the forecasts initialized daily at 00:00 UTC and 12:00 UTC using the hourly forecasts from +1 to
215 +12h. HRES forcing data is processed from the forecasts initialized at 00:00 UTC and 12:00 UTC also
216 using the forecasts from +1h to 12h. The same downwelling fluxes as in ERA5 are used but for HRES
217 we processed 2-meters temperature and dewpoint temperature and 10-meters wind-speed. Specific
218 humidity was then calculated from 2-meters temperature and dewpoint temperature. HRES also has
219 the lowest model level data archived, but due to data storage and access constraints it was more
220 efficient to process the 2-meters temperatures and 10-meters wind speed. Despite the difference in
221 the processing of the near-surface fields, lowest model level and 2-meters temperature and
222 10-meters winds are very similar, and this is not expected to impact substantially the results. In
223 ERA5 and HRES, the +1h to +12h hourly forecasts were concatenated to generate continuous time
224 series and the data processed in the original resolution was bilinearly interpolated to a regular grid
225 of $0.25^\circ \times 0.25^\circ$ and $0.1^\circ \times 0.1^\circ$. From the forecast initialized at 00:00 UTC, HRES is also available up to
226 10-d ahead. HRES forecast step frequency is hourly up to time step 90, 3-hourly from time-step 93 to
227 144 and 6-hourly from time-step 150 to 240 (i.e. 10 days). While the original 3-hourly time steps are
228 used up to day 6 (time step 144), the 6-hourly time steps from day 6 to 10 are interpolated to 3-hourly
229 frequency.

230 2.4. Experimental setup

231 Table I presents the different experiments evaluated in this study. LDAS-Monde is first forced
232 by ERA5 from 2008 to October 2018 (LDAS-ERA5) and HRES (LDAS-HRES) from April 2016 to
233 December 2018 over a western Europe domain (defined as longitudes from 10.5°W to 20.5°E ,
234 latitudes from 42°N to 59°N). IFS is obtained from frequently updated versions of operational
235 system at ECMWF (including changes in spatial and vertical resolutions, data assimilation,
236 parameterizations, and sources of data), while reanalysis like ERA5 guarantees a higher level of
237 consistency (e.g., same model) over long time period because of its frozen configuration. From April
238 2016 onward, IFS has a spatial resolution of about $0.1^\circ \times 0.1^\circ$ (HRES). Despite the spatial resolution,
239 ERA5 being a recently released dataset, its production cycle (IFS Cycle 41r2) is still close to that of the
240 HRES (IFS Cycle 41r2 to 43r3 from 2016 and 45r1 from June 2018). At the ERA5 spatial resolution,
241 large scale, long time experiments are computationally affordable, and HRES can be used to focus on
242 specific domains or events.

243 Vegetation outputs from this set of 4 experiments (assimilation of SSM and LAI as well as their
244 model counterpart, i.e. open-loops without assimilation) are then evaluated. Vegetation from
245 another experiment (model only, without assimilation) is evaluated: ISBA forced by ERA5
246 down-scaled to HRES spatial resolution (from $0.25^\circ \times 0.25^\circ$ to $0.10^\circ \times 0.10^\circ$) for 1 year (2017).
247 Additionally to the LDAS-HRES analysis experiment, daily forecast experiments with 8-day lead
248 time (from LDAS-HRES analyzed initial conditions) were also performed over 2018. Forecast
249 experiments with 2 days and 8 days lead time (LDAS_fc_2d and LDAS_fc_8d, respectively) are
250 evaluated.

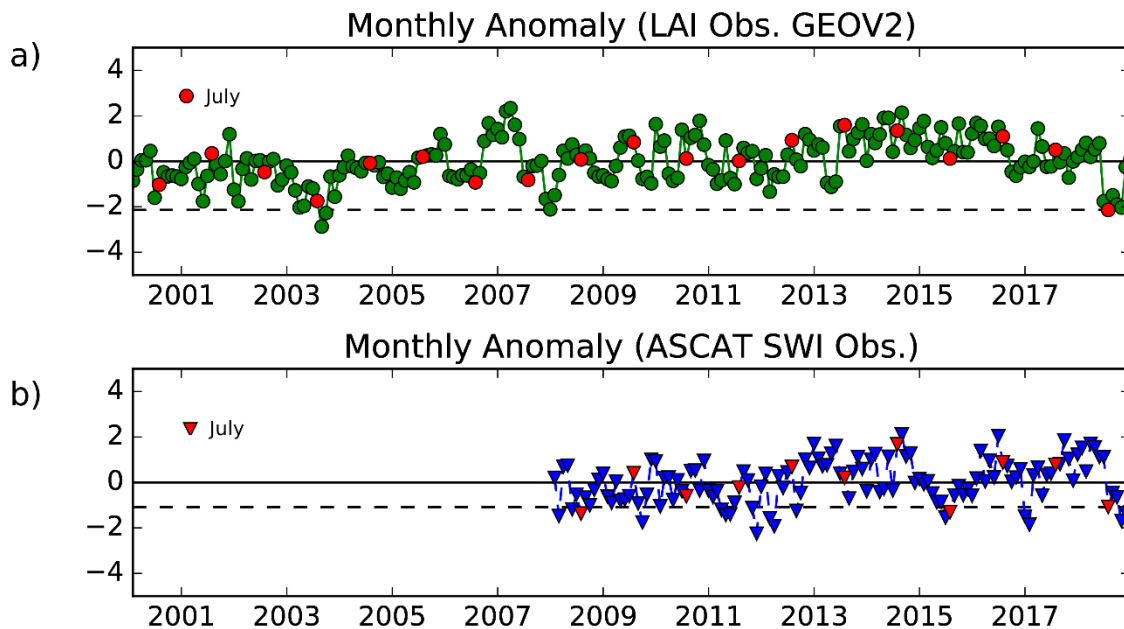
251 3. Results

252 3.1. Monitoring the heatwave impact on LAI and SSM using remote sensing

253 Time-series on figure 1 illustrate monthly anomalies (difference to the mean scaled by the
254 standard deviation) for CGLS products GEOV2 LAI (fig.1a) and ASCAT SSM (fig.1b) over the
255 periods 2000 to 2018 and 2008 to 2018, respectively, averaged over the domain (presented by figure
256 2). On both time-series, July is highlighted in red and the dashed lines represent the value of July
257 2018. As for LAI (fig.1a), July 2018 exhibits a large negative anomaly, greater than twice standard
258 deviations (stdv) on average. Such a low value is not observed in this 19-yr time-series for a month of
259 July and only one month, in summer 2003: August 2003 presents an anomaly value below than that
260 of July 2018. In 2003, large parts of Europe were affected by record-breaking temperature in summer
261 (e.g., [72]). June to October 2018 presented negative LAI anomalies, also. Table II presents the

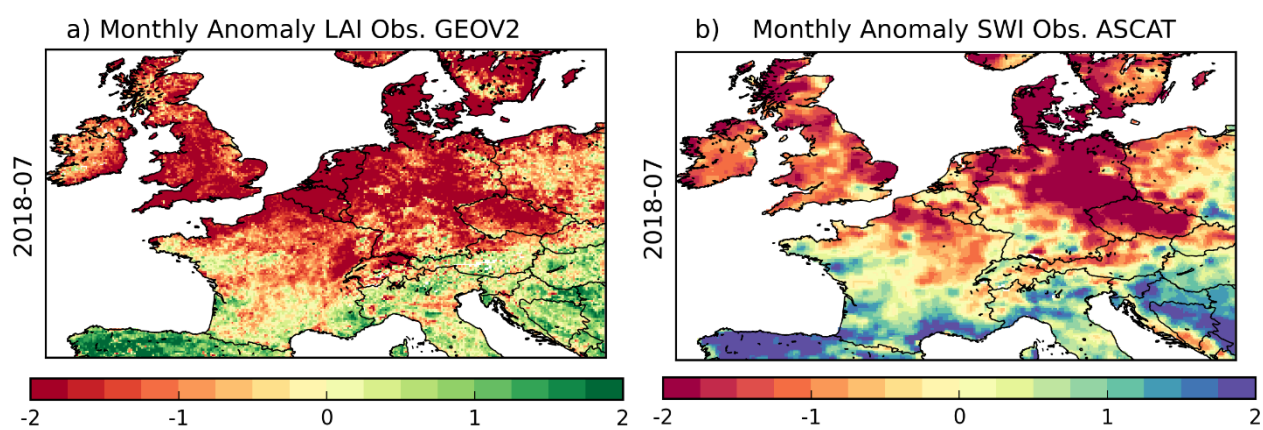
262 fraction of the considered domain affected by negative anomalies greater than 2 stdv for all months
 263 of July over 2000-2018 for GEOV2 LAI and 2008-2018 for ASCAT SSM. In July 2018, it represents
 264 nearly 19% of the domain for LAI, the largest percentage observed in 19-yr. Not only the 2018
 265 summer heatwave lead to very large negative anomaly values in LAI but it has affected a large part
 266 of the domain. Figure 2a shows maps of anomaly for July 2018 for GEOV2 LAI.

267 From fig.2a, it is visible that most of the UK, Northern part of France, Belgium, Netherlands,
 268 Denmark, Germany and Czech-republic present anomaly values greater than -2 stdv. ASCAT SSM
 269 exhibits large negative anomalies for July 2018 (fig.2b), greater than -1, also. Such low values were
 270 also observed in July 2008 and 2015, and it is worth noticing from Table II that in July 2018, 10% of
 271 the domain was affected by anomalies greater than -2 stdv, while only 2.2% and ~3% for July 2008
 272 and 2015. From fig.2b (maps on anomaly for July 2018 for ASCAT SSM), it is visible that the southern
 273 part of the domain present large positive anomaly values (e.g., north of Spain, in the Balkans) as well
 274 as the good geographical agreement between GEOV2 LAI and ASCAT SSM anomalies. While some
 275 winter months show large negative anomaly in ASCAT SSM, e.g. December 2010, 2011, this might be
 276 related to frozen conditions not accounted for and interpreted as dry conditions.



277

278 **Figure 1.** Monthly Anomaly time-series (scaled by the standard deviation) of satellite derived (a)
 279 GEOV2 Leaf Area Index over 2000-2018 and (b) Surface Soil Moisture over 2008-2018 from the
 280 Copernicus Global Land Service averaged over the domain (presented by figure 2). Months of July
 281 are highlighted in red, dashed lines represent values for July 2018.



282

283

284

285

Figure 2. Monthly anomalies (scaled by standard deviation, expressed in units of standard deviation) maps for July 2018 for (a) GEOV2 Leaf Area Index with respect to 2000-2018 and (b) Surface Soil Moisture with respect to 2008-2018 from the Copernicus Global Land Service.



286

287 **Table II:** Percentage of the domain with monthly anomalies lower than -2 stdv for satellite derived GEOV2 Leaf Area Index, ASCAT surface
288 soil moisture. Only months of July are represented.

	July 2000	July 2001	July 2002	July 2003	July 2004	July 2005	July 2006	July 2007	July 2008	July 2009	July 2010	July 2011	July 2012	July 2013	July 2014	July 2015	July 2016	July 2017	July 2018
GEOV2 Leaf Area Index	5	0.4	0.25	5	0.6	0.8	1.84	1.14	0.22	0.03	0.67	0.70	0.28	0.7	0.25	2	0.10	0.6	18.8
ASCAT SWI	N/A	N/A	N/A	N/A	N/A	N/A	N/A	N/A	N/A	2.2	0.04	1.75	0.17	1.5	0.5	0.06	3.02	0.01	10.

289

290 3.2. Monitoring the heatwave impact on vegetation using LDAS-Monde

291 LDAS-Monde being an offline reanalysis of the land surface variables, it is forced by
292 atmospheric datasets: ERA5 and HRES in this study. Using both datasets to force LDAS-Monde
293 produces a long reanalysis of the LSVs (from the use of ERA5) with real-time and even forecast
294 capacity (from the use of HRES). As ERA5 is available with a large temporal extent (from 2000 at the
295 time of study) it offers the possibility to analyze climatic signals. Anomaly time-series of air
296 temperature and precipitation from ERA5 are presented in figure 3. While it is not our intention to
297 repeat the study from [49] on predicting the summer 2018 heatwave it is however interesting to
298 highlight that the April to August period in 2018 exhibits rather large positive anomaly values of air
299 temperature (fig.3a) with July 2018 being the highest value observed between January 2001 and
300 October 2018. For precipitation, all months from May to October 2018 present large negative
301 anomalies with July 2018 being the third lowest within the considered period. One may also note the
302 coherence between air temperature and precipitation from ERA5 and the satellite derived
303 observation presented above for this 2018 heatwave event, particularly for LAI. As seen from figures
304 3 and 1a, large positive anomalies of air temperature are associated with large negative anomalies of
305 precipitation as well as large negative anomalies of LAI. In the beginning of 2007 temperature and
306 precipitation show positive anomalies which reflect on LAI presenting large positive anomalies.
307 While in the beginning of 2013, both air temperature and LAI show negative anomalies.

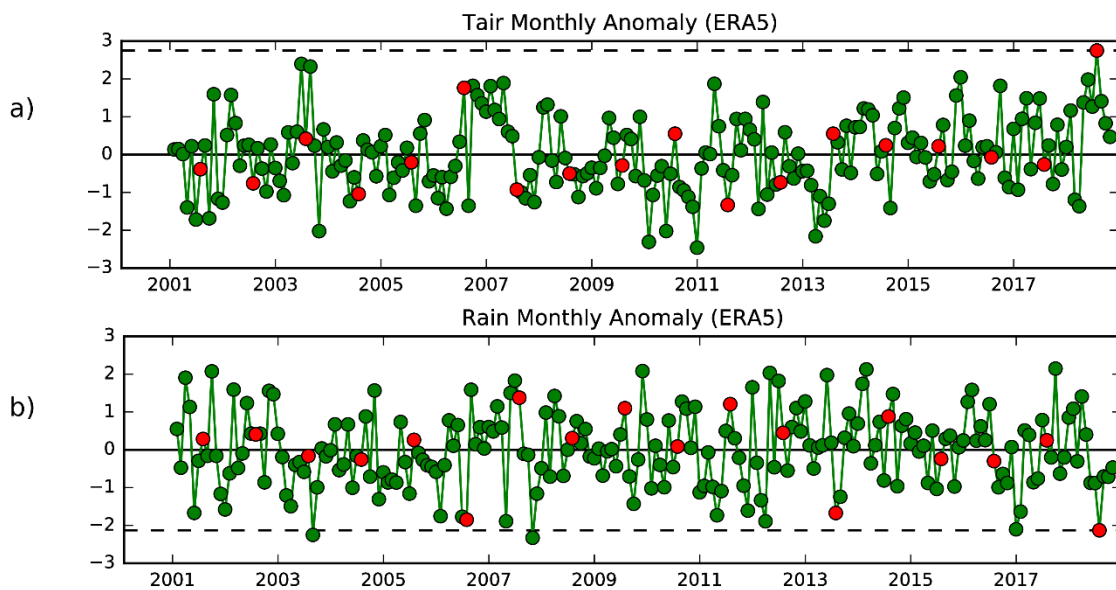
308 When LDAS-Monde is driven by ERA5 and integrates LAI and SSM through data assimilation,
309 those anomalies should be reflected on analyzed land surface conditions and their impact
310 propagated to other land surface variables through biophysical processes and feedbacks in the
311 model. Figure 4a illustrates observed CGLS GEOV2 Leaf Area Index (LAI), over 2008-2018 as well as
312 LDAS-Monde LAI time-series forced by either ERA5 (LDAS-ERA5 hereafter) over January
313 2008-October 2018 or HRES (LDAS-HRES hereafter) over April 2016-December 2018. Figure 4b
314 shows the same as fig.4a for the common April 2014 to October 2018 period. From figure 4 one may
315 notice the good agreement between the analyzed LAI and the observed annual cycle. While neither
316 the open-loop nor the analysis capture the maximum LAI peak well (as already observed by [18]),
317 the analysis efficiently corrects for the open-loop delay during the senescence phase. Considering
318 the period where both ERA5 and HRES are available to force LDAS-Monde (April-2016 to October
319 2018), one may notice the relative good agreement between LDAS-ERA5 and LDAS-HRES, both in
320 the open-loops and analyses. The senescence phase being remarkably picked-up by LDAS-HRES
321 analysis (which failed capturing the LAI peak intensity though).

322 Upper panel of figure 5 illustrates seasonal RMSD (fig5.a) and correlation (fig5.b) values
323 between LAI from the model forced by either ERA5 (LDAS-ERA5 Open-loop) or HRES
324 (LDAS-HRES Open-loop), the analysis forced by either ERA5 (LDAS-ERA5 Analysis) or HRES
325 (LDAS-HRES Open-loop) and GEOV2 LAI estimates from CGLS from April 2016 to October 2018.
326 Figure 5 lower panel shows the same between modelled/analyzed soil moisture from the second
327 layer of soil (1-4cm) and ASCAT surface soil moisture estimates from CGLS, also (and converted into
328 the model space, in m^3m^{-3} , as detailed in section 2.1). From figure 5 (all panels), one may see that
329 LDAS-ERA5 and LDAS-HRES open-loops are quite comparable, LDAS-HRES open-loop being
330 slightly better than LDAS-ERA5 open-loop in representing both LAI and soil moisture. It is also
331 visible that the analyses add skill to both open-loops for both variables, which indicates the healthy
332 behavior from the land data assimilation system. Over the whole common period (from April 2016
333 to October 2018), averaged R and RMSD values for LDAS-ERA5 open-loop (analysis) are
334 0.575(0.798) and $1.215 \text{ m}^2\text{m}^{-2}$ ($0.796 \text{ m}^2\text{m}^{-2}$) for LAI, 0.748(0.772) and $0.038 \text{ m}^3\text{m}^{-3}$ ($0.035 \text{ m}^3\text{m}^{-3}$) for soil
335 moisture, respectively. For LDAS-HRES, they are 0.601(0.808) and $1.150 \text{ m}^2\text{m}^{-2}$ ($0.772 \text{ m}^2\text{m}^{-2}$) for LAI
336 and 0.750(0.772), $0.038 \text{ m}^3\text{m}^{-3}$ ($0.036 \text{ m}^3\text{m}^{-3}$), respectively.

337 Finally, figure 6 shows LAI for the month of July 2018 from the open-loop, observations,
338 analysis as well as LAI differences (analysis minus open-loop) for LDAS-ERA5 (upper panels,
339 $0.25^\circ \times 0.25^\circ$ spatial resolution) and LDAS-HRES (lower panels, $0.10^\circ \times 0.10^\circ$ spatial resolution). From
340 the two open-loops, one can see that LDAS-ERA5 and LDAS-HRES overestimate LAI with respect to

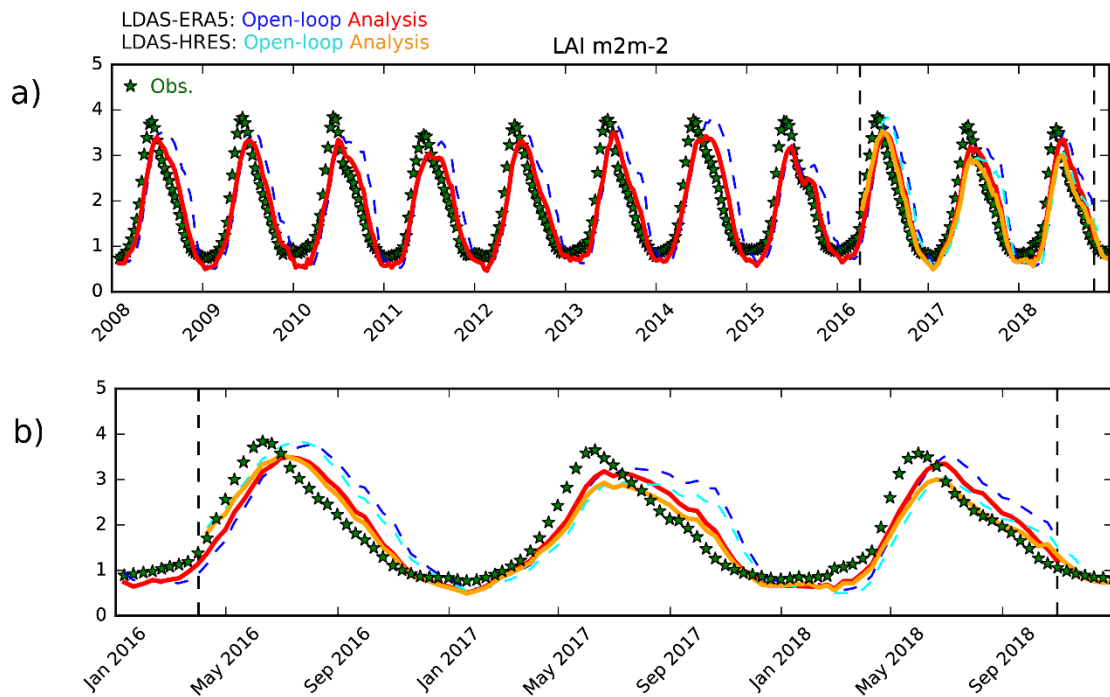
341 the observations. LDAS-HRES open-loop is however in better agreement with the observations than
 342 LDAS-ERA5 open-loop, particularly over the area most affected by the heatwave (e.g. over Belgium,
 343 the Netherlands, Germany and Poland). While the assimilation is efficiently reducing LAI in both
 344 LDAS-ERA5 and LDAS-HRES analyses, the latter is in better agreement with the observations than
 345 LDAS-ERA5 analysis, also. Despite their spatial resolution differences, ERA-5 and HRES results
 346 present similar LAI patterns. They both underestimate the amplitude and spatial extent of the
 347 drought in the open-loop, and for both the analysis effectively improves the particular LAI
 348 conditions associated to the 2018 heatwave. Furthermore, due to the large-scale nature of the
 349 drought event the spatial resolution differences between ERA5 and HRES do not affect significantly
 350 the simulations.

351 Figure 7 represents maps of monthly anomaly from LDAS-ERA5 for July 2008, 2010, 2012, 2014,
 352 2016 and 2018 for soil moisture in the fourth layer of soil (wg4, between 20 cm and 40cm) as well as
 353 drainage, runoff and evapotranspiration over most of the UK. While wg4 is one of the control
 354 variables (i.e. directly impacted by the analysis), drainage, runoff and evapotranspiration are only
 355 indirectly impacted by the analysis through model feedbacks. July 2018 presents the strongest
 356 negative anomalies. It is worth mentioning the positive anomaly values for July 2012, particularly in
 357 runoff and drainage responding to persistent rain during the first weekend of July that had led to
 358 flooding in many part of the UK
 359 (<https://www.metoffice.gov.uk/learning/learn-about-the-weather/weather-phenomena/case-studies/july-2012-flooding>, last access January 2019).
 360



361

362 **Figure 3:** Monthly Anomaly time-series (scaled by the standard deviation, expressed in units of
 363 standard deviation) of air temperature (a) and precipitations from ERA5 atmospheric reanalysis
 364 dataset over January 2001 – October 2018.



365

366

367

368

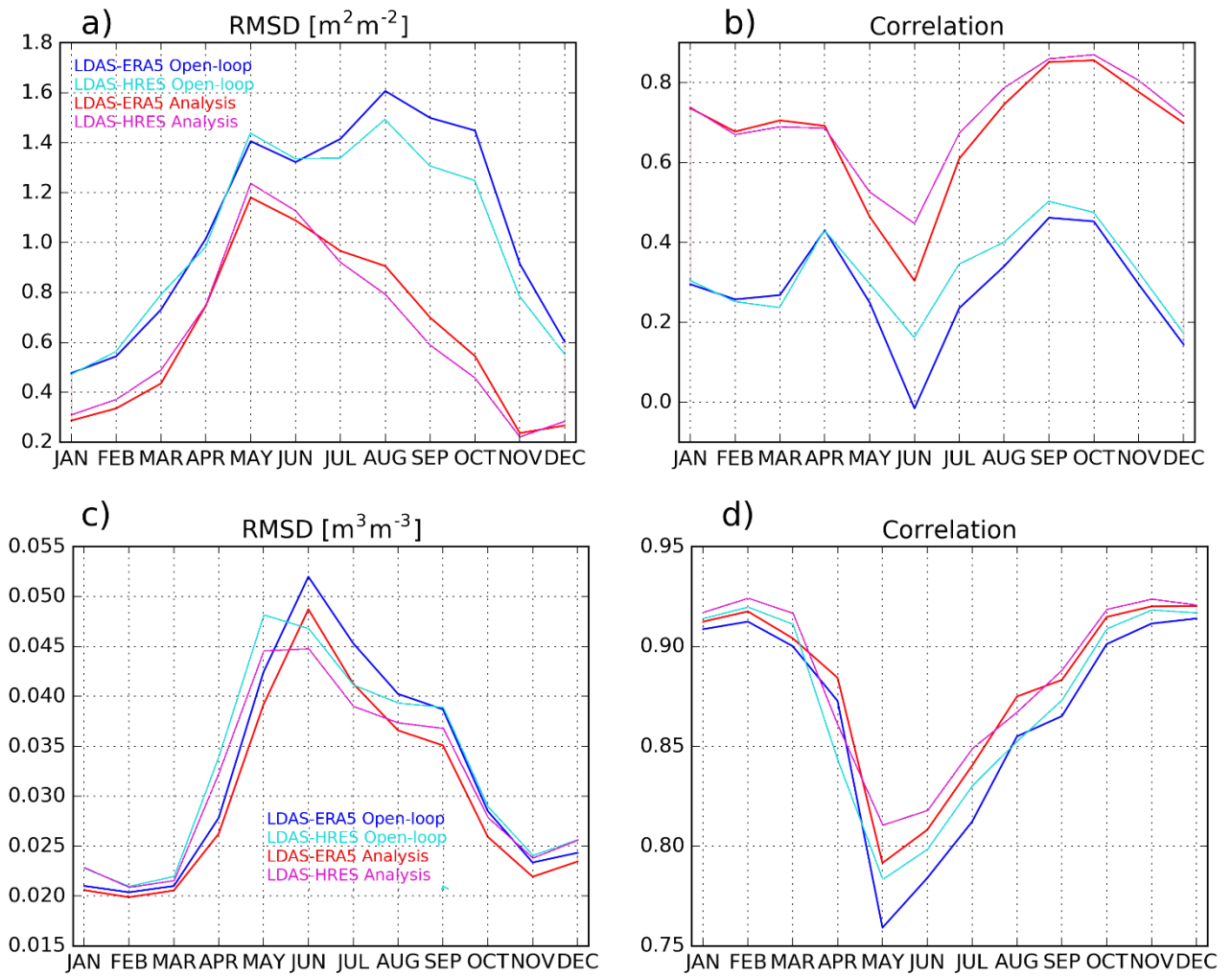
369

370

371

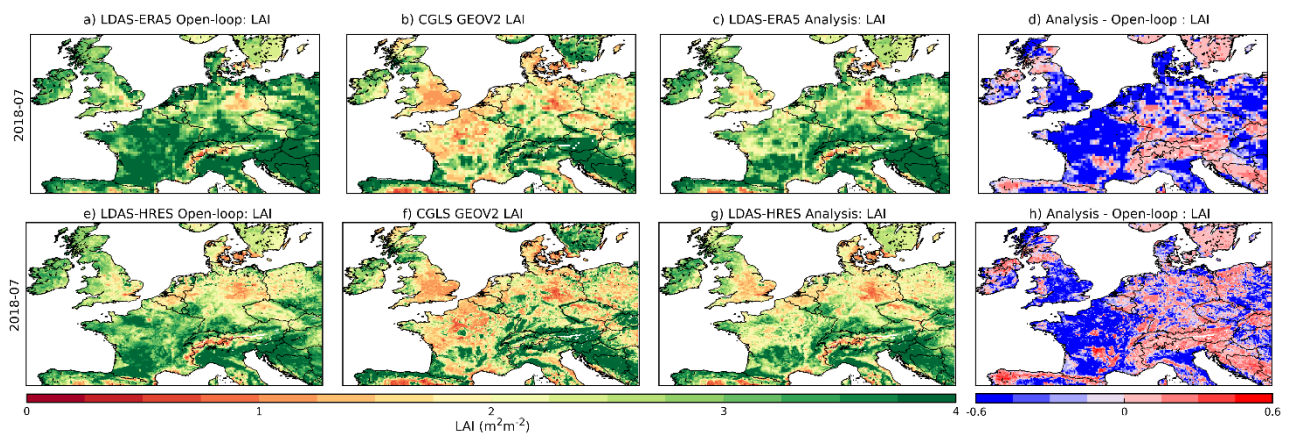
372

Figure 4. a) Observed CGLS GEOV2 Leaf Area Index (LAI) (green stars) over January 2008 to December 2018 as well as LDAS-Monde LAI time-series forced by either ERA5 (Open-loop is in blue, analysis is in red) over January 2008–October 2018 or HRES (Open-loop is in cyan, analysis is in orange) over April 2016–December 2018. b) Same as a) over LDAS-HRES and LDAS-ERA5 common period (April 2016 to October 2018). Data are averaged over the domain illustrated by figure 2, dashed line represents the date from when HRES is available (April 2016) and the date up to when ERA5 is available (at the time of the study).



373
374
375
376
377
378
379
380

Figure 5: Upper panel, seasonal (a) RMSD and (b) correlation values between leaf area index (LAI) from the model forced by either ERA5 (LDAS-ERA5 Open-loop in blue) or HRES (LDAS-HRES Open-loop in cyan), the analysis forced by either ERA5 (LDAS-ERA5 Analysis in red) or HRES (LDAS-HRES Open-loop in pink) and GEOV2 LAI estimates from the Copernicus Global Land Service project from 04/2016 to 10/2018. Lower panel, same as upper panel between modelled/analyzed soil moisture from the second layer of soil (1-4cm) and ASCAT surface soil moisture estimates from the Copernicus Global Land Service project.

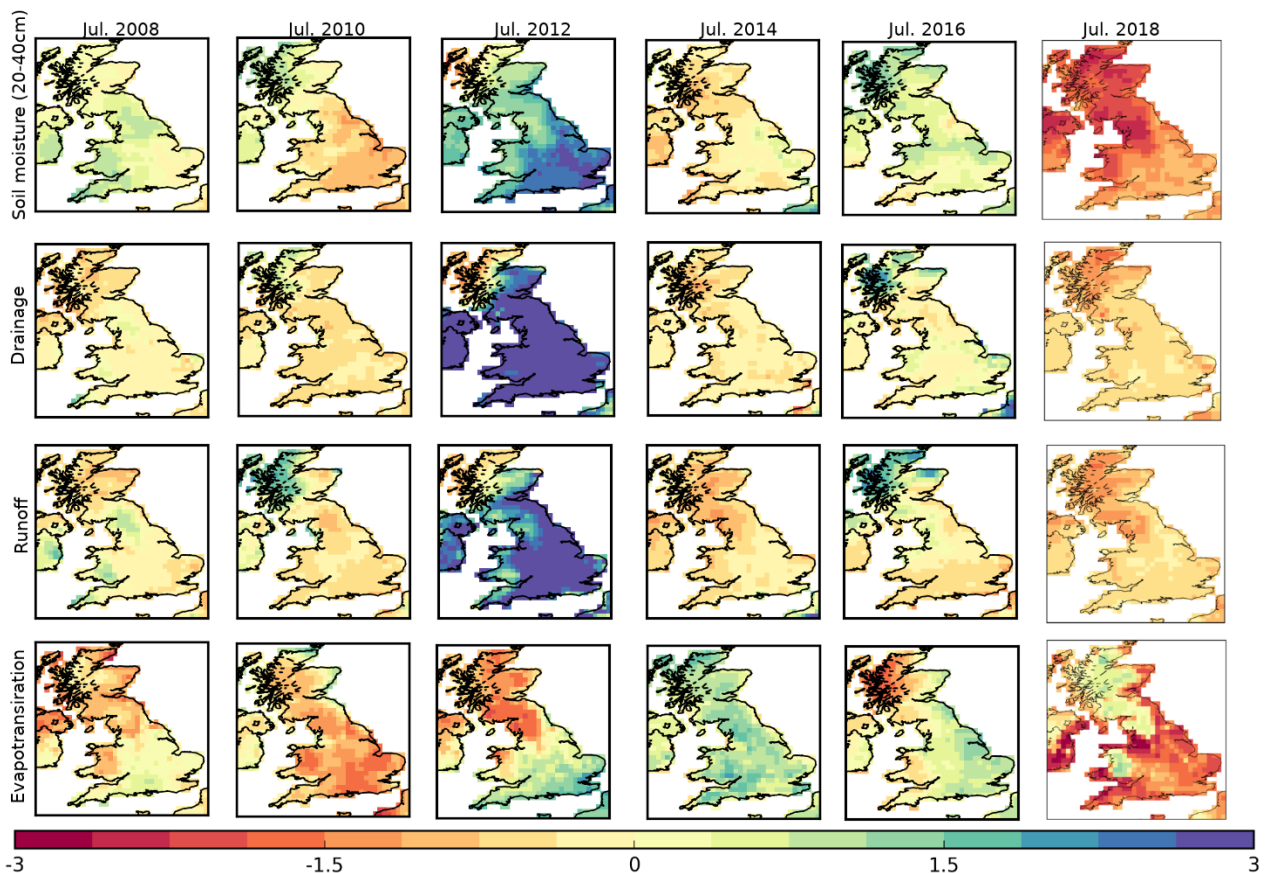


381
382
383

Figure 6: Upper panel, Leaf Area Index from (a) LDAS-ERA5 Open-loop, (b) the observations, (c) LDAS-ERA5 Analysis and (d) differences between LDAS-ERA5 Analysis and LDAS-ERA5

384
385

Open-loop for July 2018. Lower panel, same as upper panel for LDAS-HRES. Spatial resolution of upper panel is $0.25^{\circ} \times 0.25^{\circ}$, spatial resolution of lower panel is $0.10^{\circ} \times 0.10^{\circ}$.



386

387

388

389

390

Figure 7. Maps of monthly anomalies (expressed in units of standard deviation) from LDAS-ERA5 analysis for July 2008, 2010, 2012, 2014, 2016 and 2018 with respect to the 2008–2018 period (from left to right) for the following variables: soil moisture from the fourth layer of soil (between 20 cm and 40cm), drainage, runoff and evapotranspiration (from top to bottom).

391

3.3. Resolution vs. System evaluation

392

393

394

395

396

397

398

399

400

401

402

403

404

405

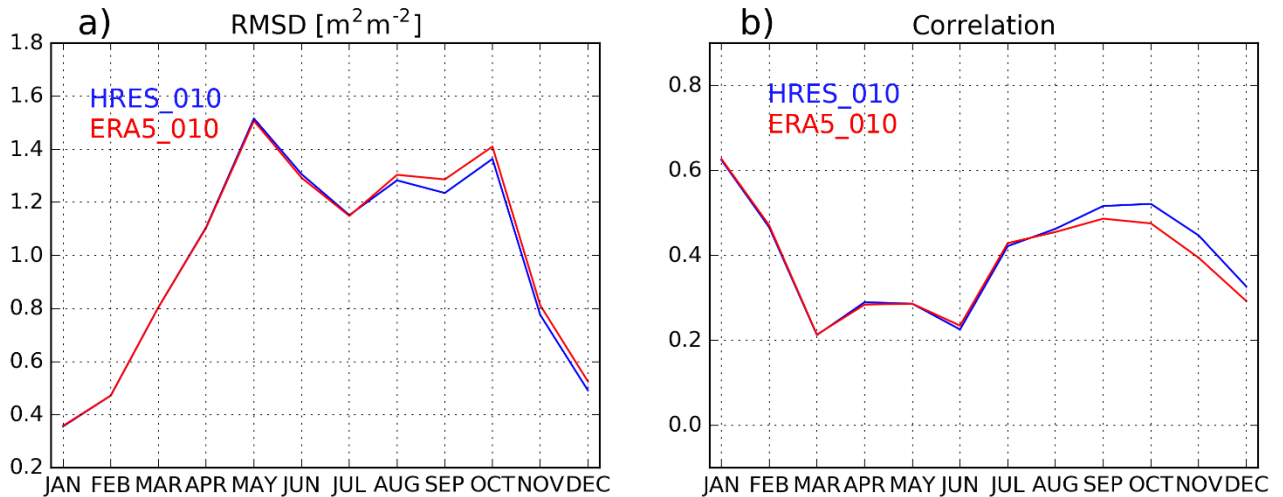
406

407

408

409

Results presented above showed that driving the LDAS by either ERA5 or HRES lead to good results monitoring the impact of the summer 2018 heatwave on vegetation, with HRES providing better results. In an attempt to investigate whether the improvement from the use of ERA5 to HRES is due to the resolution only (e.g. better representation of land cover) or to the forcing quality (or both), another experiment was carried out for 2017 (see Table I). ERA5 was downscaled from $0.25^{\circ} \times 0.25^{\circ}$ to $0.10^{\circ} \times 0.10^{\circ}$ (ERA5_010) spatial resolution to force ISBA and outputs were compared to those of LDAS_HRES open-loop (ran for 2017, with similar initial conditions). A bilinear interpolation from the native grid to the regular grid was made. Figure 8 illustrates monthly scores (R and RMSD values over 2017) for LAI from 2 experiments, namely ERA5_010 and LDAS_HRES open-loop. From the two panels of figure 8, one may appreciate the score similarities between ERA5_010 and LDAS_HRES open-loop. The later only performs slightly better than ERA5_010 from July onward for both R and RMSD values. HRES was upscaled to ERA5 spatial resolution to run ISBA and outputs where compared to those of LDAS-ERA5 open-loop (ran for 2017, with similar initial conditions), also, and similar results as discussed above were obtained (not shown). Although a longer time period would be required to further test these configurations, it is very interesting to notice than when ERA5 forcing is downscaled to $0.10^{\circ} \times 0.10^{\circ}$ to force ISBA, it performs almost as good as the operational forcing, HRES. These results could justify running longer periods of time of ERA5 at $0.10^{\circ} \times 0.10^{\circ}$ when the operational forcing is not available (e.g., prior to April 2016).



410

411

412

413

Figure 8: Monthly (a) RMSD and (b) correlation values between leaf area index (LAI) from the model forced by either HRES_010 or ERA5_010 (ERA5 forcing down-scaled to HRES spatial resolution) and GEOV2 LAI estimates from the Copernicus Global Land Service project for the year 2017.

414

4. Discussions

415

416

417

418

419

420

421

422

423

424

425

Both LDAS-Monde configurations forced by either ERA5 or HRES lead to an accurate representation of vegetation during the summer 2018 heatwave and in general. The HRES configuration presents slightly better results over the common period investigated. HRES being obtained from frequently updated versions of the IFS it is not a fixed system in time, while a reanalysis like ERA5 guarantees a higher level of consistency because of its frozen configuration. ERA5 has a coarser spatial resolution than the HRES. Its spatial resolution allows however LDAS experiments to be long term and affordable at large scale. With ERA5 available back to 1950 and covering near real-time needs with the ERA5T (<https://climate.copernicus.eu/climate-reanalysis>), an LDAS-ERA5 would be able to provide a model climate as reference for anomalies of the land surface conditions. Significant anomalies could then be used to trigger more detailed monitoring and forecasting activities for a region of interest using, for example the LDAS-HRES.

426

4.1. Are LAI and SSM relevant indicators?

427

428

429

430

431

432

433

434

435

436

437

438

439

The Summer 2018 heatwave clearly had an impact on vegetation and soil moisture, as seen using satellite derived estimates of LAI and SSM. Those satellite estimates are very useful to monitor extreme events impacts but their use is limited by their temporal frequency of a few days at best. While microwave remote sensing provides a way to quantitatively describe the water content of a shallow near-surface soil layer, [73], the variable of interest for applications in short- and medium-range meteorological modeling and hydrological studies over vegetated areas is the root-zone soil moisture content which controls e.g. plant transpiration [68]. Similarly, estimates of above-ground biomass might be more useful than LAI for application linked to agriculture. Integration of these satellite derived datasets into LSMs through data assimilation is therefore of paramount importance to improve monitoring accuracy of extreme events impacts on LSVs. Not only the representation of LAI and SSM in such system will be improved but other model variables will benefit from the assimilation through biophysical processes and feedbacks in the model too [7, 10, 18, 74].

440

4.2. Can the impact of heat waves on vegetation be anticipated?

441

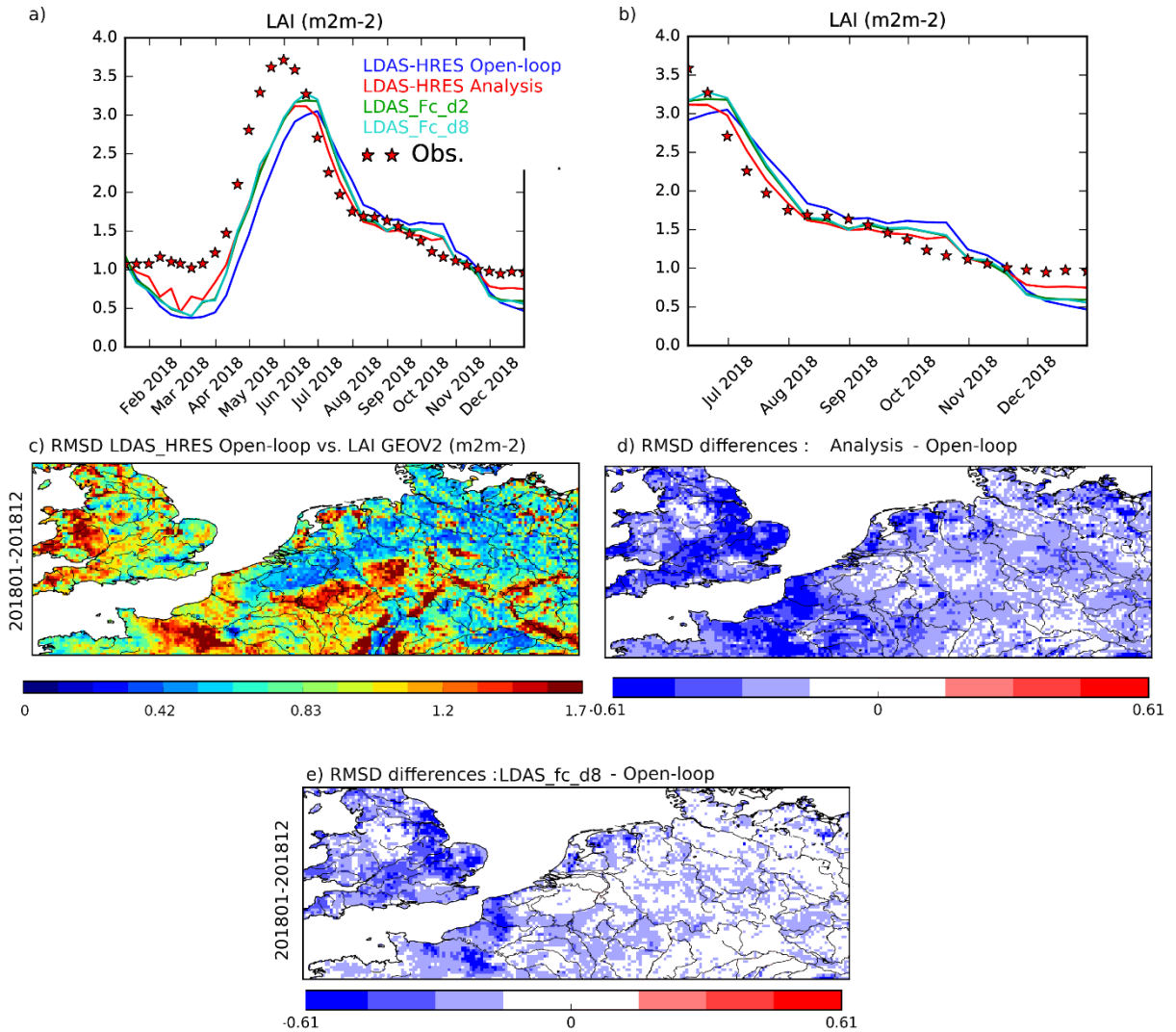
442

443

Two other experiments are presented in order to (i) study the possibility of forecasting the impact of extreme events on vegetation few days in advance and (ii) highlighting the fact that a forecast initialized by an analyzed state can have more skills than an open loop. For the whole 2018

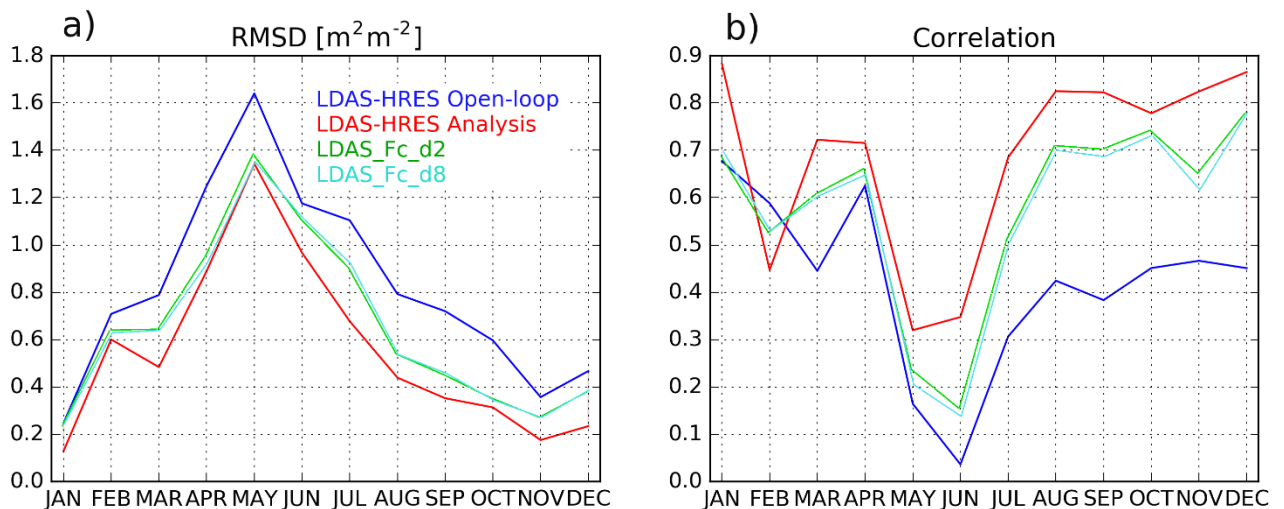
444 and for each daily analysis from LDAS-HRES, 2 forecast experiments (2-day and 8-day forecast, see
445 Table I) were conducted. The atmospheric forcing forecast is coming from HRES, as described in the
446 materials and methods sections. For the sake of clarity, only forecasts with lead time of 2 and 8 days
447 are presented (LDAS_fc_d2 and LDAS_fc_d8, respectively). Figure 9a illustrates LAI time-series
448 from the open-loop, the analysis (ran for 2018, only) as well as the 2 forecast experiments
449 (LDAS_fc_d2 and LDAS_fc_d8) for 2018 averaged over a domain defined as: longitudes from 4°W to
450 15°E and latitudes from 48°N to 55°N. According to figure 2, this domain was more severely affected
451 by the heatwave, and is represented by figure 9c. Firstly, the large error between all the experiments
452 and the observations for the start of the growing season is noticeable. From March to June
453 LDAS_HRES analysis as well as LDAS_fc_d2 and LDAS_fc_d8 are only slightly correcting for this
454 issue. This is a known issue as already mentioned by [18], the CO₂ –responsive version of ISBA is
455 such that during the growing phase, enhanced photosynthesis corresponds to a CO₂ uptake, which
456 results in vegetation growth from a prescribed LAI minimum threshold (1 m²m⁻² for coniferous
457 forest or 0.3 m²m⁻² for other vegetation types). These thresholds are probably too low and are
458 currently being revisited using the CGLS LAI long term dataset. This is expected to lead to better
459 representation of LAI during the vegetation growing phase [75]. However, during the senescence
460 phase (see zoom on figure 9b), the analysis is quite efficient in reducing the differences with the
461 observed LAI and it is quite interesting to notice that so are the 2-d and 8-d forecasts of LAI
462 initialized by the analysis. This suggests that the impact of assimilating satellite observations in
463 LDAS-Monde has the capacity to mitigate model deficiencies, leading to better estimates of the
464 system states and that this impact can last in time. From all panels of figure 9, one may see that
465 LDAS_fc_d2 and LDAS_fc_d8 are closer to the observations than the open-loop. Figure 9c represents
466 RMSD values between the open-loop (ran for 2018, only) and the LAI GEOV2 observations and
467 figure 9d the RMSD differences between the open-loop (analysis) and the LAI GEOV2. Negative
468 (blue) values indicate areas where the analysis has smaller (i.e. better) RMSD values than the
469 open-loop. Figure 9d is dominated by negative (blue) values showing the added value of the
470 analysis over the open-loop. Finally figure 9e presents RMSD differences between the open-loop
471 (LDAS_fc_d8) and the LAI GEOV2 observations and it is very interesting to notice than an 8-day
472 forecast initialized by an analysis presents better skills in capturing LAI than an open-loop for most
473 of the domain.

474 This result is emphasized by figure 10 showing monthly RMSD and R values between LAI from
475 the 4 above-mentioned experiments (LDAS-HRES open-loop and analysis, LDAS_fc_d2 and
476 LDAS_fc_d8) and the GEOV2 observations over 2018. The RMSD and R values from LDAS_fc_d2
477 and LDAS_fc_d8 experiments are better than from the open-loop, all year long. They are closer to
478 those from the LDAS-HRES analysis than from its open-loop counterpart. As seen on figure 10b, it is
479 from July 2018 that the differences between the open-loop and the analysis are the strongest. Impact
480 of assimilating LAI and SSM estimates has a time persistence of at least 8 days on LAI. Future work
481 could focus on giving more statistical strength to those results in particular by considering a longer
482 time period as well as looking at other LSVs.



483
 484
 485
 486
 487
 488
 489
 490

Figure 9. (a) LAI time series from the model (LDAS-HRES Open-loop in blue), the analysis (LDAS-HRES Analysis in red), the 2-d and 8-d forecasts from the analysis (LDAS_Fc_d2 in green , LDAS_Fc_d8 in cyan respectively) as well as the observations from the Copernicus Global Land Service (LAI GEOV2, red stars) for 2018. (b) same as (a) focusing on the June-December period.(c) RMSD values between LDAS-HRES Open-loop ran over 2018 and LAI GEOV2, (d) RMSD differences between LDAS-HRES Analysis (Open-loop) and LAI GEOV2, (e) same as (d) for LDAS_fc_d8 and Open-loop.



491

492

493

494

Figure 10. Monthly (a) RMSD and (b) R values between LAI from the model (LDAS-HRES open-loop in blue), analysis (LDAS-HRES Analysis in red), the 2-d and 8-d forecast experiments initialised by the analysis and the Copernicus Global Land Service LAI GEOV2 over 2018.

495

5. Conclusions and perspectives

496

497

498

499

500

501

502

503

504

505

506

507

508

509

510

511

512

513

514

515

516

517

518

519

520

521

522

523

524

525

526

This study has investigated the capability of LDAS-Monde offline land data assimilation system to represent the impact of the summer 2018 heatwave on vegetation. Satellite derived leaf area index and surface soil moisture were assimilated in LDAS-Monde forced by either ERA5 reanalyses (0.25°x0.25° spatial resolution) or the IFS HRES operational product (0.10°x0.10° spatial resolution) from ECMWF. Both analysis experiments were able to represent the impact of the heatwave on vegetation well. While there is a surface physiography and modeling advantage of the HRES configuration, there is added value in down-scaling ERA5 to HRES spatial resolution, too. It would allow consistent, long term and high-resolution reanalysis of the LSVs. The possibility of forecasting LSVs was successfully implemented and it was showed that a forecast of LAI from analyzed initial conditions has more skills than an open-loop (with a persistence of at least 8 days). Combining ERA5 atmospheric re-analysis, HRES analysis and its forecast within LDAS-Monde is highly relevant to foster research for land applications at various timescales from daily to annual. The use of HRES data to force LDAS-Monde is very promising and it can be complemented by ECMWF 51-member ensemble forecasts (~18 km spatial resolution). Moreover, one member of the ensemble is similar to HRES at a coarser spatial resolution, and as the ensemble is available up to 15-days lead time (twice a day and up to 45 days twice a week) it can be used to test longer range forecast of LSVs than when using HRES. Use of the ECMWF ensemble in LDAS-Monde could help capturing uncertainties in the representation of LSVs. It would open the possibility to anticipate the impact of heatwaves at monthly temporal scales using a probabilistic method.

One of the limitations to the use of the discussed land data assimilation system at a high spatial resolution, for example using grid cells of 1 km or 300 m, is that analyzed atmospheric forcings are not available at these scales. While downscaling atmospheric forcing like the IFS HRES (e.g. from 0.1°x0.1° to 0.01°x0.01° spatial resolution) is likely to add uncertainties, their impact on the representation of the LSVs can be reduced through the dynamic integration of satellite-derived LAI observations at fine scale like the 300m spatial resolution product from Copernicus Global Land Service. For the meteorological forcing, the use of AROME (Application de la Recherche à l'Opérationnel à Méso-Échelle) operational numerical prediction model from Météo-France atmospheric variables to drive the LDAS could also be investigated as its spatial resolution is already of 1.3 km x 1.3 km over France. The process of comparing Land Surface Models and observations, e.g. through data assimilation, permits highlighting model deficiencies, also. It is likely that the model would benefit from new LAI minimal values parameterization that are currently

527 being revisited at Météo-France using the long-term CGLS data-set including more than 18-yr of LAI
528 data.

529

530 **Author Contribution:** Conceptualization, Clément Albergel; Investigation, Clément Albergel;
531 Methodology, Clément Albergel, Emanuel Dutra and Gianpaolo Balsamo; Writing – original draft,
532 Clément Albergel; Writing – review & editing, Clément Albergel, Emanuel Dutra, Bertrand Bonan,
533 Yongjun Zheng, Simon Munier, Gianpaolo Balsamo, Patricia de Rosnay, Joaquin Munoz-Sabater and
534 Jean-Christophe Calvet.

535

536 **Acknowledgments:** Results were generated using the Copernicus Climate Change Service
537 Information, 2017. The Authors would like to thanks the Copernicus Global Land Service for
538 providing the satellite derived Leaf Area Index and Surface Soil Moisture

539

Conflicts of interest: The authors declare no conflict of interest

540 References

- 541 1. Balsamo, G., Albergel, C., Beljaars, A., Boussetta, S., Brun, E., Cloke, H., Dee, D., Dutra, E., Muñoz-Sabater,
542 J., Pappenberger, F., de Rosnay, P., Stockdale, T., and Vitart, F.: ERA-Interim/Land: a global land surface
543 reanalysis data set, *Hydrol. Earth Syst. Sci.*, 19, 389-407, <https://doi.org/10.5194/hess-19-389-2015>, 2015.
- 544 2. Balsamo, G., Agusti-Panareda, A., Albergel, C. et al., Satellite and in situ observations for advancing global
545 Earth surface modelling: a review, 2018 accepted *Remote Sens.*, remotesensing-380225
- 546 3. Schellekens, J., Dutra, E., Martínez-de la Torre, A., Balsamo, G., van Dijk, A., Sperna Weiland, F., Minvielle,
547 M., Calvet, J.-C., Decharme, B., Eisner, S., Fink, G., Flörke, M., Peßenteiner, S., van Beek, R., Polcher, J.,
548 Beck, H., Orth, R., Calton, B., Burke, S., Dorigo, W., and Weedon, G. P.: A global water resources ensemble
549 of hydrological models: the earthH2Observe Tier-1 dataset, *Earth Syst. Sci. Data*, 9, 389-413,
550 <https://doi.org/10.5194/essd-9-389-2017>, 2017.
- 551 4. Dirmeyer, P. A., Gao, X., Zhao, M., Guo, Z., Oki, T., and Hanasaki N.: The Second Global Soil Wetness
552 Project (GSWP-2): Multi-model analysis and implications for our perception of the land surface, *B. Am.*
553 *Meteorol. Soc.*, 87, 1381–1397, <https://doi.org/10.1175/BAMS-87-10-1381>, 2006.
- 554 5. Reichle, R. H., R. D. Koster, P. Liu, S. P. P. Mahanama, E. G. Njoku and M. Owe: Comparison and
555 assimilation of global soil moisture retrievals from the Advanced Microwave Scanning Radiometer for the
556 Earth Observing System (AMSR-E) and the Scanning Multichannel Microwave Radiometer (SMMR). *J.*
557 *Geophys. Res.* 112 (D9): D09108 (10.1029/2006JD008033), 2007.
- 558 6. Lahoz, W., and De Lannoy, G.; Closing the gaps in our knowledge of the hydrological cycle over land:
559 conceptual problems, *Survey of Geophysics*, 2014, 35, 577-606.
- 560 7. Albergel, C.; Munier, S.; Bocher, A.; Bonan, B.; Zheng, Y.; Draper, C.; Leroux, D.J.; Calvet, J.-C.
561 LDAS-Monde Sequential Assimilation of Satellite Derived Observations Applied to the Contiguous US:
562 An ERA5 Driven Reanalysis of the Land Surface Variables. *Remote Sens.* 2018b, 10, 1627.
- 563 8. de Rosnay, P., et al., A simplified Extended Kalman Filter for the global operational soil moisture analysis
564 at ECMWF. *Quarterly Journal of the Royal Meteorological Society*, 2013. 139(674): p. 1199-1213.
- 565 9. de Rosnay, P., Balsamo, G., Albergel, C., Muñoz-Sabater, J. and Isaksen, L.: Initialisation of land surface
566 variables for numerical weather prediction, *Surv. Geophys.*, 35, 607–621, 2014.
- 567 10. Kumar, S. V., Jasinski, M., Mocko, D., Rodell, M., Borak, J., Li, B., Kato Beaudoin, H., and Peters-Lidard, C.
568 D.: NCA-LDAS land analysis: Development and performance of a multisensor, multi-variate land data
569 assimilation system for the National Climate Assessment, *J. Hydrometeor.*,
570 <https://doi.org/10.1175/JHM-D-17-0125.1>, online first, 2018.
- 571 11. Massari, C.; Camici, S.; Ciabatta, L.; Brocca, L. Exploiting Satellite-Based Surface Soil Moisture for Flood
572 Forecasting in the Mediterranean Area: State Update Versus Rainfall Correction. *Remote Sens.* 2018, 10,
573 292.
- 574 12. Bauer, P., Thorpe ,A. and Brunet, G.: The quiet revolution of numerical weather prediction. *Nature* 525,
575 47-55, doi:10.1038/nature14956, 2015.
- 576 13. Koster, R. D., Mahanama, S. P. P., Livneh, B., Lettenmaier, D. P., and Reichle, R. H., Skill in streamflow
577 forecasts derived from large-scale estimates of soil moisture and snow, *Nature Geoscience Letters*, 2010, 3,
578 613-616.

- 579 14. Bierkens, M., and van Beek, L., Seasonal predictability of European discharge: Nao and hydrological
580 response time, *Journal of Hydrometeorological*, 2009, 10, 953-968.
- 581 15. Schlosser, A., and Dirmeyer, P., Potential predictability of Eurasian snow cover. *Atmospheric Sciences*
582 *Letters*, 2001, 2(1-4), 1-8.
- 583 16. Bamzai, A. and Shukla, J., Relation between Eurasian snow cover, snow depth and the Indian summer
584 monsoon: An observational study, *Journal of climate*, 1999, 12, 3117-3132.
- 585 17. Lettenmaier, D. P., D. Alsdorf, J. Dozier, G. J. Huffman, M. Pan, and E. F. Wood: Inroads of remote sensing
586 into hydrologic science during the WRR era, *Water Resour. Res.*, 51, 7309–7342,
587 doi:10.1002/2015WR017616, 2015.
- 588 18. Albergel, C., Munier, S., Leroux, D. J., Dewaele, H., Fairbairn, D., Barbu, A. L., Gelati, E., Dorigo, W.,
589 Faroux, S., Meurey, C., Le Moigne, P., Decharme, B., Mahfouf, J.-F., and Calvet, J.-C.: Sequential
590 assimilation of satellite-derived vegetation and soil moisture products using SURFEX_v8.0: LDAS-Monde
591 assessment over the Euro-Mediterranean area, *Geosci. Model Dev.*, 10, 3889-3912,
592 <https://doi.org/10.5194/gmd-10-3889-2017>, 2017.
- 593 19. Rodell, M., P. R. Houser, U. Jambor, J. Gottschalck, K. Mitchell, C.-J. Meng, K. Arsenault, B. Cosgrove, J.
594 Radakovich, M. Bosilovich, J. K. Entin, J. P. Walker, D. Lohmann, and D. Toll, The Global Land Data
595 Assimilation System, *Bull. Amer. Meteor. Soc.*, 85(3), 381–394, 2004.
- 596 20. Kaminski et al., Assimilating atmospheric data into a terrestrial biosphere model: A case study of the
597 seasonal cycle. *Global Biogeochemical cycles*, 2002, 16(1).
- 598 21. Sawada, Y., and T. Koike, Simultaneous estimation of both hydrological and ecological parameters in an
599 ecohydrological model by assimilating microwave signal, *J. Geophys. Res. Atmos.*, 119,
600 doi:10.1002/2014JD021536, 2014.
- 601 22. Sawada, Y., T. Koike, and J. P. Walker, A land data assimilation system for simultaneous simulation of soil
602 moisture and vegetation dynamics, *J. Geophys. Res. Atmos.*, 120, doi: 10.1002/2014JD022895, 2015.
- 603 23. Lievens, H., et al., SMOS soil moisture assimilation for improved hydrologic simulation in the Murray
604 Darling Basin, Australia. *Remote Sensing of Environment*, 2015. 168: p. 146-162.
- 605 24. de Lannoy G.J.M., de Rosnay P., Reichle R.H. (2015) Soil Moisture Data Assimilation. In: Duan Q.,
606 Pappenberger F., Thielen J., Wood A., Cloke H., Schaake J. (eds) *Handbook of Hydrometeorological*
607 *Ensemble Forecasting*. Springer, Berlin, Heidelberg.
- 608 25. Pinnington, E., T. Quaipe, and E. Black, Impact of remotely sensed soil moisture and precipitation on soil
609 moisture prediction in a data assimilation system with the JULES landsurface model. *Hydrology and*
610 *Earth System Sciences*, 2018. 22(4): p. 2575-2588.
- 611 26. de Lannoy, G. J. M., R. H. Reichle, K. R. Arsenault, P. R. Houser, S. Kumar, N. E. C. Verhoest, and V. R. N.
612 Pauwels: Multiscale assimilation of Advanced Microwave Scanning RadiometerEOS snow water
613 equivalent and Moderate Resolution Imaging Spectroradiometer snow cover fraction observations in
614 northern Colorado. *Water Resources Research*, 48 (1), doi:10.1029/2011WR010588, w01522, 2012.
- 615 27. Kumar, S., C. Peters-Lidard, K. Arsenault, A. Getirana, D. Mocko, and Y. Liu, 2015: Quantifying the added
616 value of snow cover area observations in passive microwave snow depth data assimilation. *J.*
617 *Hydrometeor.*, 16, 1736–1741, doi:10.1175/JHM-D-15-0021.1.
- 618 28. Kumar, S., and Coauthors, 2014: Assimilation of remotely sensed soil moisture and snow depth retrievals
619 for drought estimation. *J. Hydrometeor.*, 15, 2446–2469, doi:10.1175/JHM-D-13-0132.1.
- 620 29. Dziubanski, D. J., and K. J. Franz, 2016: Assimilation of AMSR-E snow water equivalent data in a
621 spatially-lumped snow model. *Journal of Hydrology*, 540, 26 – 39, doi: <https://doi.org/10.1016/j.jhydrol.2016.05.046>.
- 622 30. Fletcher, S. J., G. E. Liston, C. A. Hiemstra, and S. D. Miller, 2012: Assimilating MODIS and AMSR-E Snow
623 Observations in a Snow Evolution Model. *Journal of Hydrometeorology*, 13 (5), 1475–1492,
624 doi:10.1175/JHM-D-11-082.1.
- 625 31. Zhang, Y.-F., T. J. Hoar, Z.-L. Yang, J. L. Anderson, A. M. Toure, and M. Rodell, 2014: Assimilation of
626 MODIS snow cover through the Data Assimilation Research Testbed and the Community Land Model
627 version 4. *Journal of Geophysical Research: Atmospheres*, 119 (12), 7091–7103, doi:10.1002/2013JD021329,
628 2013JD021329.
- 629 32. Barbu, A. L., Calvet, J.-C., Mahfouf, J.-F., Albergel, C., and Lafont, S.: Assimilation of Soil Wetness Index
630 and Leaf Area Index into the ISBA-A-gs land surface model: grassland case study, *Biogeosciences*, 8, 1971–
631 1986, doi:10.5194/bg-8-1971-2011, 2011.
- 632

- 633 33. Barbu, A.L., J.-C. Calvet, J.-F. Mahfouf, and S. Lafont: Integrating ASCAT surface soil moisture and
634 GEOV1 leaf area index into the SURFEX modelling platform: a land data assimilation application over
635 France. *Hydrol. Earth Syst. Sci.*, 18, 173–192, doi:10.5194/hess-18-173-2014, 2014.
- 636 34. Fairbairn, D., Barbu, A. L., Napoly, A., Albergel, C., Mahfouf, J.-F., and Calvet, J.-C.: The effect of
637 satellite-derived surface soil moisture and leaf area index land data assimilation on streamflow
638 simulations over France, *Hydrol. Earth Syst. Sci.*, 21, 2015–2033, <https://doi.org/10.5194/hess-21-2015-2017>,
639 2017.
- 640 35. Leroux, D.J.; Calvet, J.-C.; Munier, S.; Albergel, C. Using Satellite-Derived Vegetation Products to Evaluate
641 LDAS-Monde over the Euro-Mediterranean Area. *Remote Sens.* 2018, 10, 1199.
- 642 36. Tangdamrongsub, N., S. C. Steele-Dunne, B. C. Gunter, P. G. Ditmar, and A. H. Weerts, 2015: Data
643 assimilation of GRACE terrestrial water storage estimates into a regional hydrological model of the Rhine
644 River basin. *Hydrology and Earth System Sciences*, 19 (4), 2079–2100, doi:10.5194/hess-19-2079-2015, URL
645 <http://www.hydrol-earth-syst-sci.net/19/2079/2015/>.
- 646 37. Kumar, S. V., and Coauthors, 2016: Assimilation of Gridded GRACE Terrestrial Water Storage Estimates
647 in the North American Land Data Assimilation System. *Journal of Hydrometeorology*, 17 (7), 1951–1972,
648 doi:10.1175/JHM-D-15-0157.1.
- 649 38. Giroto, M., G. J. M. De Lannoy, R. H. Reichle, and M. Rodell (2016), Assimilation of gridded terrestrial
650 water storage observations from GRACE into a land surface model, *Water Resour. Res.*, 52, 4164–4183, doi:
651 10.1002/2015WR018417.
- 652 39. Fairbairn, D., Barbu, A.L., Mahfouf, J.-F., Calvet, J.-C., and Gelati, E.: Comparing the ensemble and
653 extended Kalman filters for in situ soil moisture assimilation with contrasting conditions, *Hydrol. Earth
654 Syst. Sci.*, 19, 4811–4830, <https://doi.org/10.5194/hess-19-4811-2015>, 2015.
- 655 40. Quintana-Segui, P., Le Moigne, P., Durand, Y., Martin, E., Habets, F., Baillon, M., Canellas, C.,
656 Franchisteguy, L., and Morel, S.: Analysis of near surface atmospheric variables: validation of the
657 SAFRAN analysis over France, *J. Appl. Meteorol. Clim.*, 47, 92–107, 2008.
- 658 41. Habets, F., Boone, A., Champeaux, J.-L., Etchevers, P., Franchisteguy, L., Leblois, E., Ledoux, E., Le
659 Moigne, P., Martin, E., Morel, S., Noilhan, J., Quintana Seguí, P., Rousset Regimbeau, F., and Vienno, P.:
660 The SAFRAN-ISBA-MODCOU hydrometeorological model applied over France, *J. Geophys. Res.*,
661 113, D06113, <https://doi.org/10.1029/2007JD008548>, 2008.
- 662 42. Dee, D. P., and Coauthors, 2011: The ERA-Interim reanalysis: Configuration and performance of the data
663 assimilation system. *Quart. J. Roy. Meteor. Soc.*, 137, 553–597, doi:10.1002/qj.828.
- 664 43. Tall, M., Albergel, C., Bonan, B., Zheng, Y., Guichard, F., Dramé, M., Thierno Gaye, A. and Calvet, J.-C.,
665 Towards a long-term reanalysis of land surface variables over western Africa: LDAS-Monde applied over
666 Burkina Faso, to be submitted to Remote Sensing.
- 667 44. Hersbach, H, de Rosnay, P, Bell, B, Schepers, D, Simmons, A, Soci, C, Abdalla, S, Alonso-Balmaseda, M,
668 Balsamo, G, Bechtold, P, Berrisford, P, Bidlot, J-R, de Boissésón, E, Bonavita, M, Browne, P, Buizza, R,
669 Dahlgren, P, Dee, D, Dragani, R, Diamantakis, M, Flemming, J, Forbes, R, Geer, AJ, Haiden, T, Hólm, E,
670 Haimberger, L, Hogan, R, Horányi, A, Janiskova, M, Laloyaux, P, Lopez, P, J., M-S, Peubey, C, Radu, R,
671 Richardson, D, Thépaut, J-N, Vitart, F, Yang, X, Zsótér, E and Zuo, H: Operational global reanalysis:
672 progress, future directions and synergies with NWP, ERA Report Series, 27, 65pp, December 2018.
- 673 45. Liu, Y.Y., Jeu, R.D., McCabe, M.F., Evans, J.P., van Dijk, A.I.J.M., 2011b. Global lon-term passive
674 microwave satellite-based retrievals of vegetation optical depth. *Geophys.Res. Lett.* 38 (18).
675 <http://dx.doi.org/10.1029/2011GL048684/abstract>.
- 676 46. Liu, Y. Y., W. A. Dorigo, R. M. Parinussa, R. A. M. De Jeu, W. Wagner, M. F. McCabe, J. P. Evans & A. I. J.
677 M. Van Dijk. Trend-preserving blending of passive and active microwave soil moisture retrievals, *Remote
678 Sens. Environ.*, 123, 280–297, doi:10.1016/j.rse.2012.03.014, 2012.
- 679 47. Dorigo, W.A., A. Gruber, R.A.M. De Jeu, W. Wagner, T. Stacke, A. Loew, C. Albergel, L. Brocca, D. Chung,
680 R.M. Parinussa and R. Kidd: Evaluation of the ESA CCI soil moisture product using ground-based
681 observations, *Remote Sensing of Environment*, <http://dx.doi.org/10.1016/j.rse.2014.07.023>, 2015.
- 682 48. Dorigo, W., Wagner, W., Albergel, C. et al.: ESA CCI Soil Moisture for improved Earth system
683 understanding: State-of-the art and future directions, *Remote Sensing of Environment*,
684 <http://dx.doi.org/10.1016/j.rse.2017.07.001>, 2017.
- 685 49. Magnusson, L., Ferranti, L. and Vamborg, F., Forecasting the 2018 European heatwave, ECMWF
686 newsletter, number 157, autumn 2018, P.4, 2018.

- 687 50. Masson, V.; Le Moigne, P.; Martin, E.; Faroux, S.; Alias, A.; Alkama, R.; Belamari, S.; Barbu, A.; Boone, A.;
688 Bouysse, F.; et al. The SURFEXv7.2 land and ocean surface platform for coupled or offline simulation of
689 earth surface variables and fluxes. *Geosci. Model Dev.* **2013**, *6*, 929–960.
- 690 51. Mahfouf, J.-F.; Bergaoui, K.; Draper, C.; Bouysse, F.; Taillefer, F.; Taseva, L. A comparison of two off-line
691 soil analysis schemes for assimilation of screen level observations. *J. Geophys. Res.* **2009**, *114*, D08105.
- 692 52. Noilhan, J.; Mahfouf, J.-F. The ISBA land surface parameterisation scheme. *Glob. Planet. Chang.* **1996**, *13*,
693 145–159.
- 694 53. Calvet, J.-C.; Noilhan, J.; Roujean, J.-L.; Bessemoulin, P.; Cabelguenne, M.; Olioso, A.; Wigneron, J.-P. An
695 interactive vegetation SVAT model tested against data from six 780 contrasting sites. *Agric. For. Meteorol.*
696 **1998**, *92*, 73–95.
- 697 54. Calvet, J.-C.; Rivalland, V.; Picon-Cochard, C.; Guehl, J.-M. Modelling forest transpiration and CO₂
698 fluxes—Response to soil moisture stress. *Agric. For. Meteorol.* **2004**, *124*, 143–156.
- 699 55. Gibelin, A.-L.; Calvet, J.-C.; Roujean, J.-L.; Jarlan, L.; Los, S.O. Ability of the land surface model ISBA-A-gs
700 to simulate leaf area index at global scale: Comparison with satellite products. *J. Geophys. Res.* **2006**, *111*,
701 1–16
- 702 56. Decharme, B., Delire, D., Minvielle, M., Colin, J., Vergnes, J.-P., Alias, A., Saint-Martin, D., Séférian, R.,
703 Sénési, S., Voldoire, A. Recent changes in the ISBA-CTRIP land surface system for use in the CNRM-CM6
704 climate model and in global off-line hydrological applications, submitted to JAMES, October 2018.
- 705 57. Dewaele, H.; Munier, S.; Albergel, C.; Planque, C.; Laanaia, N.; Carrer, D.; Calvet, J.-C. Parameter
706 optimisation for a better representation of drought by LSMs: Inverse modelling vs. sequential data
707 assimilation. *Hydrol. Earth Syst. Sci.* **2017**, *21*, 4861–4878.
- 708 58. Boone, A.; Masson, V.; Meyers, T.; Noilhan, J. The influence of the inclusion of soil freezing on simulations
709 by a soil vegetation–atmosphere transfer scheme. *J. Appl. Meteorol.* **2000**, *39*, 1544–1569.
- 710 59. Decharme, B.; Martin, E.; Faroux, S. Reconciling soil thermal and hydrological lower boundary conditions
711 in land surface models. *J. Geophys. Res.-Atmos.* **2013**, *118*, 7819–7834.
- 712 60. Faroux, S.; Kaptue Tchuenta, A.T.; Roujean, J.-L.; Masson, V.; Martin, E.; Le Moigne, P. ECOCLIMAP-II/
713 Europe: A twofold database of ecosystems and surface parameters at 1 km resolution based on satellite
714 information for use in land surface, meteorological and climate models. *Geosci. Model Dev.* **2013**, *6*, 563–
715 582.
- 716 61. Calvet, J.-C.; Soussana, J.-F. Modelling CO₂-enrichment effects using an interactive vegetation SVAT
717 scheme. *Agric. For. Meteorol.* **2001**, *108*, 129–152.
- 718 62. Lafont, S.; Zhao, Y.; Calvet, J.-C.; Peylin, P.; Ciais, P.; Maignan, F.; Weiss, M. Modelling LAI, surface water
719 and carbon fluxes at high-resolution over France: Comparison of ISBA-A-gs and ORCHIDEE. *Biogeosciences* **2012**, *9*, 439–456.
- 720 63. Szczypta, C.; Calvet, J.-C.; Maignan, F.; Dorigo, W.; Baret, F.; Ciais, P. Suitability of modelled and remotely
721 sensed essential climate variables for monitoring Euro-Mediterranean droughts. *Geosci. Model Dev.* **2014**,
722 *7*, 931–946.
- 723 64. Bonan, B., Albergel, C., Zheng, Y., Barbu, A.L., Fairbairn, D., Munier S. and Calvet, J.-C., An Ensemble
724 Kalman Filter for the joint assimilation of surface soil moisture and leaf area index within LDAS-Monde:
725 application over the Euro-Mediterranean basin. Submitted to HESSD, special issue on Hydrological cycle
726 in the Mediterranean.
- 727 65. Rüdiger, C.; Albergel, C.; Mahfouf, J.-F.; Calvet, J.-C.; Walker, J.P. Evaluation of Jacobians for Leaf Area
728 Index data assimilation with an extended Kalman filter. *J. Geophys. Res.* **2010**, *115*, D09111.
- 729 66. Wagner, W., Lemoine, G., and Rott, H.: A method for estimating soil moisture from ERS scatterometer and
730 soil data, *Remote Sens. Environ.*, **70**, 191–207, 1999.
- 731 67. Bartalis, Z., Wagner, W., Naeimi, V., Hasenauer, S., Scipal, K., Bonekamp, H., Figa, J., and Anderson, C.:
732 Initial soil moisture retrievals from the METOP-A advanced Scatterometer (ASCAT), *Geophys. Res. Lett.*,
733 *34*, L20401, doi: 10.1029/2007GL031088, 2007.
- 734 68. Albergel, C., Rüdiger, C., Pellarin, T., Calvet, J.-C., Fritz, N., Froissard, F., Suquia, D., Petitpa, A., Pignatelli, B.,
735 and Martin, E.: From near-surface to root-zone soil moisture using an exponential filter: an assessment of
736 the method based on in-situ observations and model simulations, *Hydrol. Earth Syst. Sci.*, **12**, 1323–1337,
737 <https://doi.org/10.5194/hess-12-1323-2008>, 2008.
- 738

- 739 69. Kidd, R., Makhmara, H., and Paulik, C.: GIO GL1 PUM SWI I1.00.pdf, 25 pp. available at:
740 [http://land.copernicus.eu/global/ products/SWI/Documents/ProductUserManual](http://land.copernicus.eu/global/products/SWI/Documents/ProductUserManual) (last access: January
741 2014), 2013.
- 742 70. Baret, F., Weiss, M., Lacaze, R., Camacho, F., Makhmarad, H., Pacholczyk, P., and Smetse, B.: GEOV1: LAI,
743 FAPAR essential climate variables and FCOVER global time series capitalizing over existing products,
744 Part 1: Principles of development and production, *Remote Sens. Environ.*, 137, 299–309,
745 doi:10.1016/j.rse.2012.12.027, 2013.
- 746 71. Verger, A., Baret, F., & Weiss, M.: Near real time vegetation monitoring at global scale. *IEEE Journal of*
747 *Selected Topics in Applied Earth Observations and Remote Sensing*, 7(8), 3473–3481, 2014.
- 748 72. Schär, C., Vidale, P. L., Lüthi, D., Frei, C., Häberli, C., Linige, M. A. and Appenzeller C., The role of
749 increasing temperature variability in European summer heatwaves, 2004, *Nature* **volume 427**, pages 332–
750 336.
- 751 73. Schmugge, T. J.: Remote Sensing of Soil Moisture: Recent Advances, *IEEE Trans. Geosci. Remote Sens.*,
752 GE21, 145–146, 1983.
- 753 74. Fox, A.M.; Hoar, T.J.; Anderson, J.L.; Arellano, A.F.; Smith, W.K.; Litvak, M.E.; MacBean, N.; Schimel, D.S.;
754 Moore, D.J.P. Evaluation of a Data Assimilation System for Land Surface Models using CLM4.5. *J. Adv.*
755 *Model. Earth Syst.* **2018**.
- 756 75. Munier, S.; Leroux, D.; Albergel, C.; Carrer, D.; Calvet, J.C. Hydrological impacts of the assimilation of
757 satellite-derived disaggregated Leaf Area Index into the SURFEX modelling platform. *Hydrol. Earth Syst.*
758 *Sci. Discuss.* **2018**. in preparation.



759 © 2018 by the authors. Submitted for possible open access publication under the
760 terms and conditions of the Creative Commons Attribution (CC BY) license
(<http://creativecommons.org/licenses/by/4.0/>).